REMOTE SENSING

Global extent and drivers of tree cover loss quantified with high-resolution satellite data

Alexandra Tyukavina[1]*, Andrew J. Poulson[1], Jeffrey Pickering[1,2], Bernard Adusei[1], Matthew C. Hansen[1], Peter Potapov[1,3], Antoine Baggett[1], Carolina Ortiz Dominguez[1], Aleksandra Mikus[1], Andre Oktaviandra[1], Svetlana Turubanova[1], Anna Komarova[1], Diana Parker[1], Amy H. Pickens[1], Viviana Zalles[1,3], Will Byrne[1], Steven Painter[1], Lauren Thomas[1,4], Arden Ireland[1,5], Yuhao He[1], Nancy Harris[3], Xiao-Peng Song[1]

Quantifying the drivers of tree cover loss globally provides a synoptic understanding of pressures on the world's forests. Existing information about tree cover loss drivers relies on maps of coarse spatial and thematic resolution. In this study, we quantified the global extent of tree cover loss in 2018 at the scale of individual disturbances and provided a comprehensive accounting of land use outcomes using a global probability sample of 600 5 × 5–kilometer blocks mapped with high-resolution (3- to 10-meter) satellite data. Out of 277 thousand square kilometers of estimated global tree cover loss, nearly a third (29.0%) was due to long-term conversion of tree cover to other land uses, including conversion of natural tree cover to pasture (15.0%), cropland (6.4%), and nontimber tree plantations (3.8%).

The world's forests are threatened by competing land uses resulting from growing population (*1*). Accurate information on the extent and drivers of forest disturbances is crucial for climate mitigation and meeting the UN's Sustainable Development Goals (*2*, *3*). Global open collections of satellite imagery (*4*) enable consistent mapping and monitoring of forests worldwide (*5*, *6*). However, definitions of "forest" and "deforestation" formulated in a presatellite era (*7*) often lead to large uncertainties in satellite-derived estimates of forest extent and change, limiting their utility for tracking success of deforestation reduction commitments (*8*). "Tree cover," defined as the presence of trees, and "tree cover loss," defined as the removal of trees, are more generic biophysical metrics for global satellite-based monitoring.

Global tree cover loss extent has been mapped annually since 2001 at 30-m spatial resolution [(*9*), with annual updates]. This global tree cover loss map [(*9*); hereafter referred to as "GTCL map"] used in a wide variety of practical applications (*10*–*12*) reports the removal of trees (>5 m tall) regardless of their type (e.g., mature or young, naturally growing or planted) or removal method (e.g., mechanical removal by humans or natural disturbances). The GTCL map does not differentiate between temporary and long-term tree removal, which is necessary for global vegetation and carbon modeling. Additionally, it fails to distinguish various drivers of tree cover loss and associated land uses (e.g., conversion to agriculture versus mining), a crucial distinction for removing deforestation from commodity supply chains.

Available global information on tree cover loss drivers (*13*, *14*) is limited by its coarse spatial resolution (1 to 10 km) and the small number of identified drivers (five to seven classes). Both global driver maps attribute all 30-m pixels of the GTCL map (*9*) within each 1- or 10-km grid cell to one dominant loss driver for all years since 2001. This obscures disturbance drivers that are not prevalent in space or time and can increase uncertainties of tree cover loss–related carbon emissions estimates. Fire is the only tree cover loss driver characterized with the same spatial extent (global), spatial resolution (30 m), and temporal resolution (annual) as the GTCL map (*15*).

In this study, we present a global-scale analysis characterizing the extent and direct drivers (*16*) of tree cover loss with high spatial resolution (3 to 10 m) satellite data (Fig. 1). Our study is sample-based (*17*), using a stratified random sample of 600 5 × 5–km blocks (fig. S1). Using the GTCL map for stratification allowed increasing sampling efficiency by focusing on areas with detected tree cover loss, and cluster sampling of blocks allowed reducing acquisition costs of PlanetScope imagery (*18*). For each sample block, we mapped the extent of tree cover loss for 2018 using commercial 3-m–resolution PlanetScope and publicly available 10-m Sentinel-2 (*19*) imagery. Subsequent land uses were identified using imagery three years after the disturbance (2019 to 2021). High-resolution satellite images allowed identification of (i) predisturbance tree cover (natural or planted), (ii) disturbance type (mechanized clearing, fires, or other natural disturbances; Fig. 2), and (iii) postdisturbance land use (e.g., pasture, cropland, mining, and infrastructure; Figs. 3 to 5), resulting in a comprehensive typology of disturbance drivers (Table 1). A statistically rigorous sample-based approach enabled estimating the global and regional area of tree cover loss with uncertainties. Area estimates and reference block maps were then used to assess the performance of GTCL map (*9*) (table S7 and figs. S4 to S7) and the best available global drivers map (*14*) (table S8 and figs. S10 and S11).

Tree cover loss extent, types, and drivers

The estimated global area of tree cover loss in 2018 was 277 ± 22 thousand km^2 (± 1 standard error). Tropical climate domain (fig. S2B) led in terms of its contribution to global tree cover loss (63.0 ± 4.1%; Fig. 1 and table S1), including tree cover loss within and outside of tropical rainforests (34.9 ± 4.8% and 28.1 ± 3.7%, respectively). Boreal, subtropical, and temperate domains contributed 14.5 ± 2.5%, 12.8 ± 2.6%, and 9.4 ± 2.6%, respectively. At the continental scale (fig. S2A), Latin America was the leading contributor (26.6 ± 3.6%), followed by South and Southeast Asia (21.6 ± 5.2%), Africa (18.2 ± 2.7%), North and East Eurasia (15.4 ± 2.7%) and North America (12.3 ± 2.9%) (Fig. 1 and table S1). The combined contribution of Europe and Australia and Oceania was around 6% (3.9 ± 1.3% and 2.1 ± 0.9%, respectively). The top countries contributing to the global tree cover loss (Fig. 1 and table S1) were Brazil (13.5 ± 2.7%), Russia (10.9 ± 2.2%), and Indonesia (9.1 ± 4.5%).

Most tree cover loss globally was from mechanical clearing (84.0 ± 2.8%), including mechanized (59.9 ± 4.0%) and manual (24.1 ± 3.1%) clearing [Fig. 2, A and B, and table S2; see (*17*) for definitions and identification criteria]. Mechanized clearing was widespread in North America, Latin America, Europe, Russia, China, and Southeast Asia, where industrial forestry and conversion to agriculture are prevalent (Fig. 2A). Manual clearing was dominant in sub-Saharan Africa, corresponding to smallholder agriculture, but it was also common in Latin America and Southeast Asia (Fig. 2B). Flooding due to dam construction is also linked to human activities (Fig. 2C), although its global contribution was minimal (<0.01%).

The second largest disturbance type was fire, contributing 12.4 ± 2.5% of global tree cover loss (Fig. 2C and table S2). Sample blocks with the largest proportion of fire-related tree cover loss, corresponding to large fires, were found in Russia and Canada (Fig. 2C); smaller forest fires occurred throughout Latin America and Africa. We did not detect any 2018 forest fires in Southeast Asia, possibly owing to the limited sample size and a low fire year in this region (*15*) following the relatively short-lasting El Niño–related drought of 2015 and 2016 (*20*).

[1]Department of Geographical Sciences, University of Maryland, College Park, MD, USA. [2]FeatureSpace.io, Auckland, New Zealand. [3]World Resources Institute, Washington, DC, USA. [4]Department of Geography, University of Colorado Boulder, Boulder, CO, USA. [5]Department of Geography, University at Buffalo, Buffalo, NY, USA. ***Corresponding author. Email: atyukav@umd.edu**

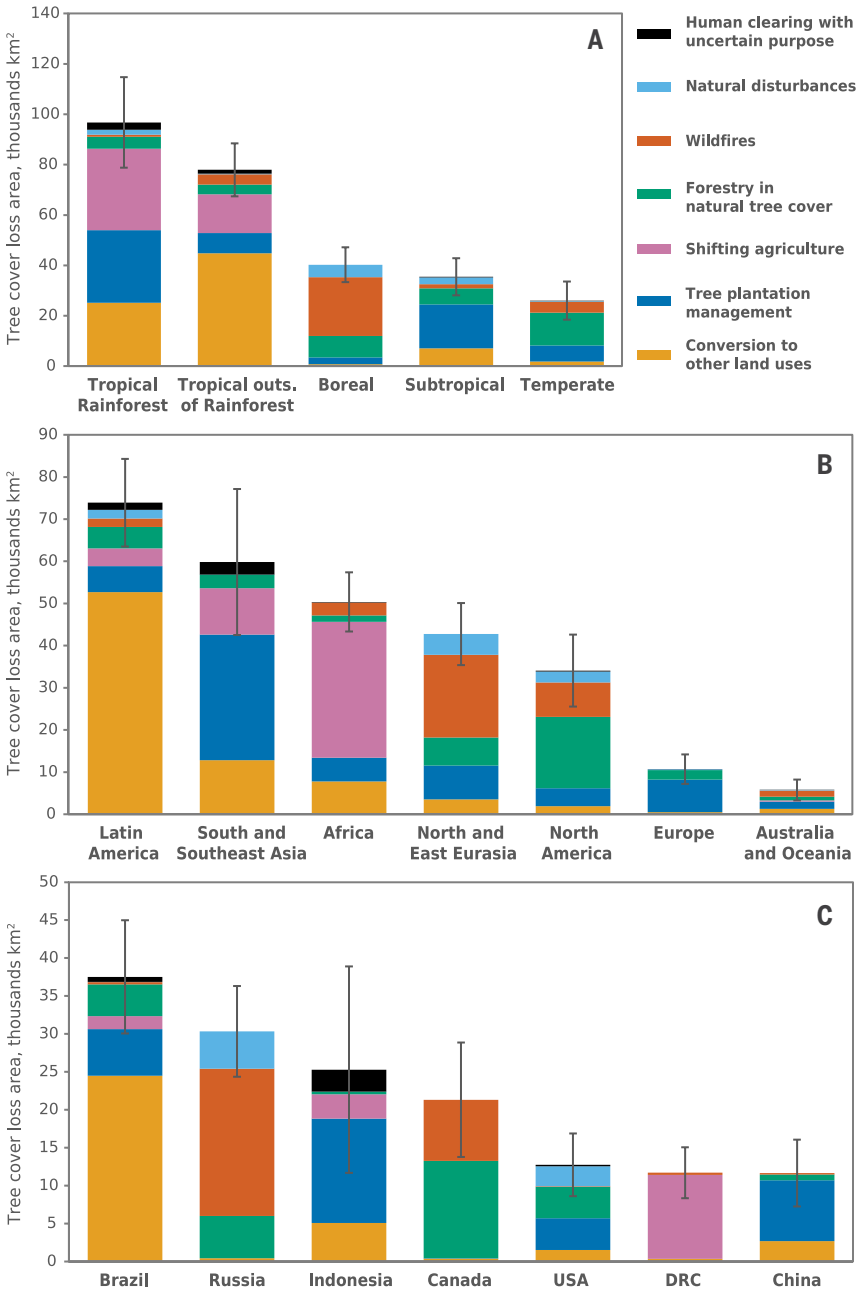

Fig. 1. Estimated area of 2018 tree cover loss. Estimated area disaggregated by combined disturbance types within climate domains (**A**), continents or regions (**B**), and top tree cover loss countries (**C**). Combined disturbance types are aggregations of the categories presented in Table 1, matching the panels of Fig. 3. Error bars represent ± 1 standard error. Boundaries of climate domains and reporting regions are presented in fig. S2. Area estimates are also presented in table S1. Outs., outside; DRC, Democratic Republic of the Congo.

Natural disturbances other than fire (Fig. 2C) formed the third disturbance type group (3.6 ± 1.4%). These include insect infestations (1.8 ± 0.9%), hurricanes and windfalls (1.7 ± 1.1%), natural flooding (0.1 ± 0.1%), and other natural disturbances of uncertain origin (<0.1%). Although the contribution of these natural disturbances to global tree cover loss was small, their share is likely to increase with climate change (*21*), and their geographic distribution has high interannual variability.

When looking at the tree cover loss drivers identified from 3 years of postdisturbance land use, we found that 29.0 ± 3.5% of global year 2018 tree cover loss was due to long-term conversion into other land uses not followed by natural tree cover regrowth (Fig. 3A and table S3). The rest represented temporary loss due to tree plantation management (22.8 ± 4.9%; Fig. 3B), shifting agriculture (17.2 ± 2.6%; Fig. 3C), forestry operations in natural tree cover (13.2 ± 2.7%; Fig. 3D), fires not followed by productive land uses ("wildfires," 12.4 ± 2.5%; Fig. 3E) and natural disturbances (3.6 ± 1.4%; Fig. 3E). These temporary loss events are followed by regrowth of the same tree cover type as before the disturbance (natural or planted) or by planted trees replacing natural tree cover within the same land use (planted clearcuts as a part of forestry land use; Fig. 3D). Although we distinguished between disturbances in natural versus planted tree cover (Fig. 3 and table S3), we did not identify from the satellite imagery whether the affected natural tree cover was old growth (i.e., mature or primary forests) or secondary owing to the difficulties of defining these categories at the global scale. In the tropics, we used an existing primary forest map (*22*) to identify that 17% of the shifting agriculture–related tree cover loss was the expansion into historically undisturbed forests (table S6) and not the reclearing of secondary regrowth, signaling the ongoing degradation of tropical forests. The hotspots of shifting agriculture expansion into tropical primary forests are the Democratic Republic of the Congo (*23*, *24*) and Borneo (fig. S3).

Within forestry operations in natural tree cover, we have distinguished clearcuts with natural regeneration (9.1 ± 2.2%), planted clearcuts (0.7 ± 0.3%), and selective logging (3.4 ± 1.0%) (Fig. 3D). The latter is typically classified as "forest degradation," implying lower carbon and biodiversity losses compared with those of clearcuts, but can lead to increased vulnerability of forests to droughts, fires, and insect infestations (*25*).

Tree cover clearing with uncertain purpose (Fig. 3F and table S3) reflects thematic uncertainty of driver attribution in our study. However, it can also be associated with land banking or grabbing practices in which the land is left without a productive land use for several years after the initial clearing with plans for future land use (*26*).

Conversion of tree cover to other land uses

Conversion of tree cover to other land uses is the most important loss category in terms of environmental consequences because it leads to the long-term replacement of trees with primarily treeless land covers. We include conversion of natural tree cover to nontimber tree plantations in the long-term conversion category, whereas planted clearcuts and management of timber and nontimber plantations are considered temporary tree cover loss. Conversion to other land uses mainly occurred in natural tree cover (27.8 ± 3.4% of the global tree cover loss) as opposed to in planted trees (1.2 ± 0.7%) (Fig. 3A and table S3). Conversion was predominantly mechanized (Fig. 5 table S5), indicating the prevalence of industrial conversion.

Pasture expansion into natural tree cover was the most widespread conversion type (15.0 ± 2.7% of the global tree cover loss; Figs. 4A and 5 and tables S4 and S5) and was concentrated almost exclusively in Latin America. Pasture gain in forested areas has been largely offset by pasture loss from conversion to croplands, with total pasture area in South America remaining stable since 2004 (*27*). Approximately

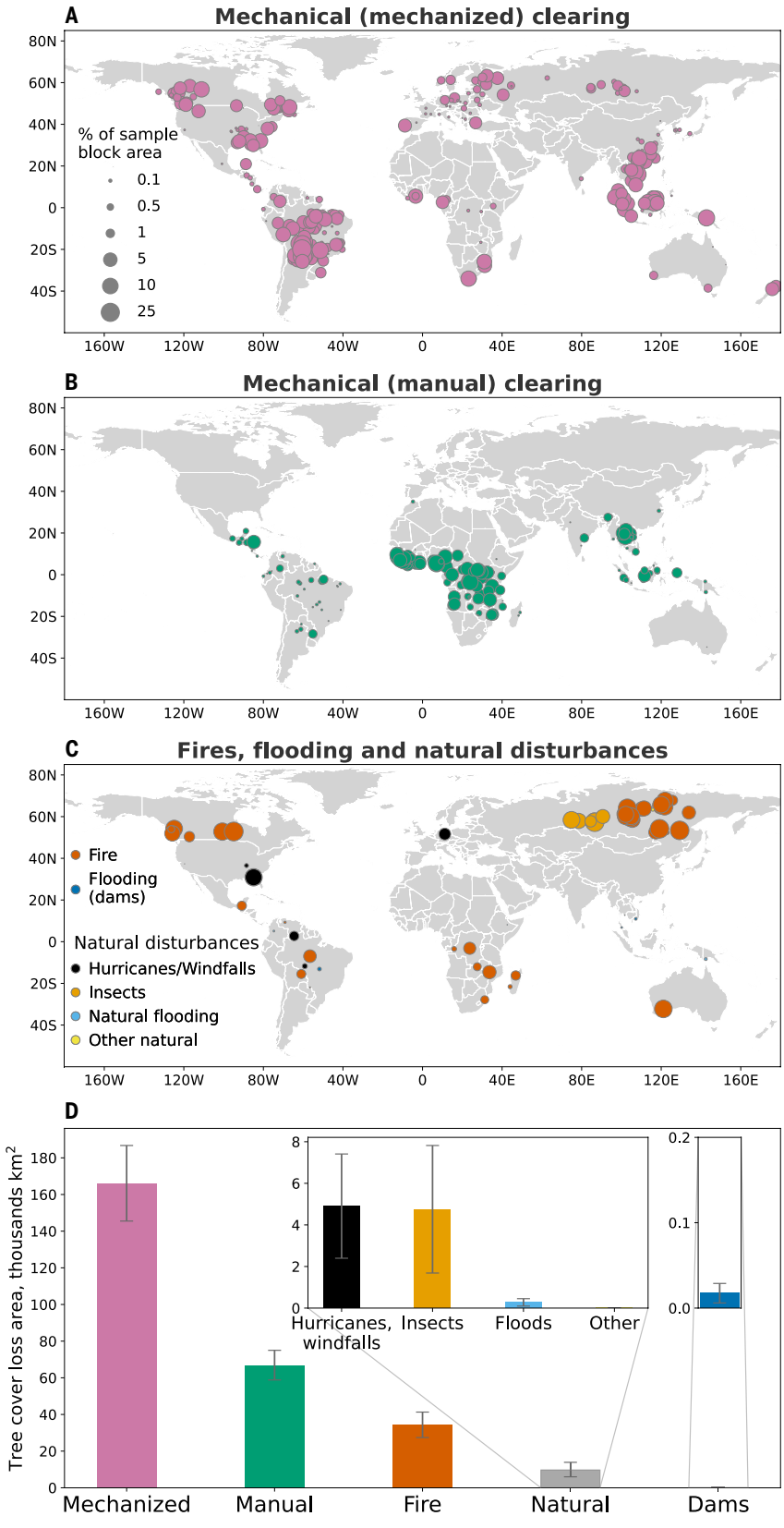

Fig. 2. Initial tree cover disturbance type identified from the satellite imagery at the time of disturbance (end of 2018). (**A** to **C**) Locations of sample blocks identified as a particular disturbance type. (**D**) Area estimates (in thousand km^2 ± 1 standard error) based on the entire sample (area estimates are also available in table S2). Disturbance types in (D) correspond to (A) and (B), except "Natural," which is a combined "Natural disturbances" class from (C). Class definitions and examples of satellite imagery are presented in (*17*).

10% of the tree cover area initially cleared for pasture may be converted into industrial croplands for export-oriented soybean production within the next 20 to 30 years (*27*).

Direct conversion of natural tree cover to cropland contributed 6.4 ± 1.5% of the global tree cover loss. It was concentrated in the dry woodlands and seasonal forests of Africa and South America (Figs. 4B and 5 and tables S4 and S5). Bolivia was a hotspot of cropland expansion into natural tree cover, mainly for industrial export-oriented monoculture soybeans (*28*). By contrast, in Africa, crop production on lands converted from natural tree cover is mostly cereals for domestic consumption rather than industrial export crops (*29*): We identified the majority of tree cover loss in Africa as manually cleared (Fig. 2B).

Conversion of natural tree cover to nontimber plantations, including palm, rubber, and tall orchards, contributed 3.8 ± 1.6% of global tree cover loss (Figs. 4C and 5 and tables S4 and S5). This driver was primarily found in Southeast Asia and West Africa, representing areas of industrial export crop cultivation. Our 2018 estimate of conversion to nontimber plantations is likely lower than that of the prior decade owing to the recent decreases in direct conversion of forests to palm and rubber plantations in Indonesia (*26*, *30*).

Other conversion drivers (Figs. 4D and 5 and tables S4 and S5) each contributed 1% or less of the total tree cover loss area and have high proportional standard errors owing to the limited global sample size. To precisely quantify these drivers, a more targeted sampling effort is needed, for example, using existing high-resolution mining and urban area datasets (*31*–*33*) for stratification. Mining and road network expansion fragment patches of natural tree cover and open them up to further disturbances and therefore are important monitoring targets.

Comparison with the GTCL map

Our estimated global area of 2018 tree cover loss agrees well with that of the GTCL map (*9*): The two estimates are within 10% (table S7). Some regional differences are explained by methodological caveats (*17*). The current study maps any tree cover loss in 2018, whereas the GTCL map (*9*) detects only the first tree cover loss event since 2001. This leads to differences in area estimates in the tropics, where tree cover regrowth is fast: In 2018, 17% of tree cover loss related to tropical shifting cultivation occurred where 2001 to 2017 tree cover loss was previously detected by the GTCL map (table S6). At least 27% of the difference between the GTCL map and the current study in the boreal region and 34% in the temperate region (table S7) can be attributed to the late-year 2017 disturbances mapped as 2018 tree cover loss in the GTCL map.

The difference in the extent of tree cover loss in boreal fires may be attributed in part to varying tree cover definitions (*17*) and in part to the GTCL map overestimating the area of complete tree removal within burn scars (fig. S9). Per-block agreement of percent tree cover loss from the GTCL map and this study is low in the boreal region and Russia (figs. S4A and S6A), where forest fires dominated tree cover loss in 2018.

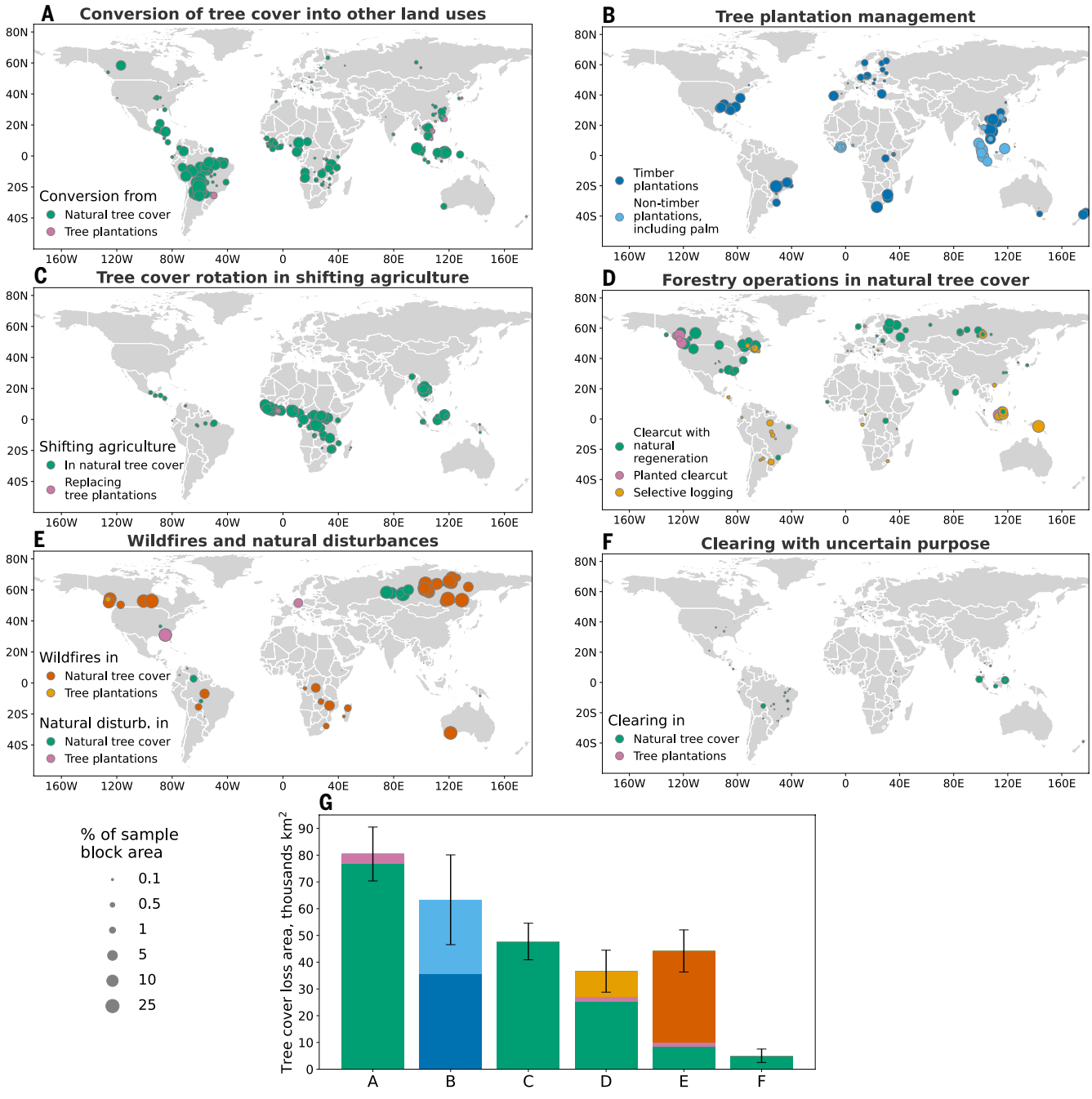

Fig. 3. Drivers of 2018 tree cover loss identified using 2019 to 2021 satellite imagery, corresponding to land use established within 3 years after the disturbance. (**A** to **F**) Locations of sample blocks identified as a particular driver. (**G**) Area estimates (in thousands km^2 ± 1 standard error) based on the entire sample (area estimates are also available in table S3). Note that (D) includes disturbances only in natural forests, (B) includes disturbances only in tree plantations, and (A), (C), (E), and (F) include both. Class definitions and examples of satellite imagery are presented in (*17*).

Very high agreement between the current study and the GTCL map (fig. S7) was observed for the sample blocks identified as mechanized conversion to pasture and cropland and as mechanized forestry, resulting in high agreement in countries and regions where mechanized clearing of tree cover is prevalent, such as Canada, the United States, and Brazil (fig. S6) as well as North America and Latin America (fig. S5). This indicates that, for characterizing mechanized tree cover clearing in these regions, the GTCL map (*9*) can be used to derive reasonably accurate area estimates through map pixel counting.

For nonmechanized clearing for shifting agriculture, the agreement between the GTCL map and the sample is low (fig. S7E), resulting in lower agreement in Africa (fig. S5A). In the Democratic Republic of the Congo, where shifting cultivation is replacing primary rainforests (fig. S3)—an easier target for satellite-based monitoring compared with secondary regrowth and drier forests—agreement between the map and this study is higher (fig. S6E). To accurately characterize small-scale, repeated tree removal within established shifting cultivation landscapes, the GTCL map could be used to guide targeted regional sampling or mapping efforts.

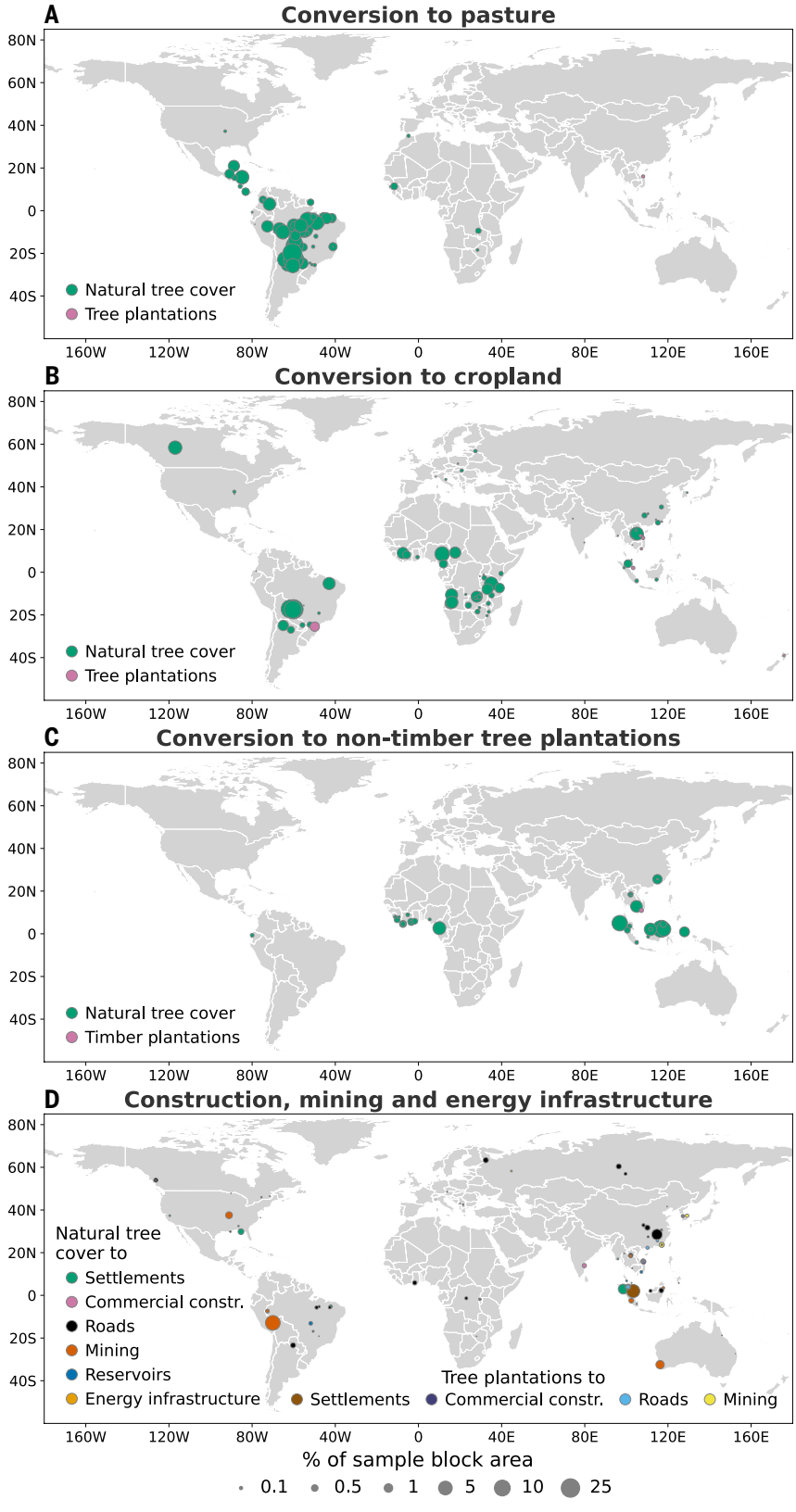

Fig. 4. Geographic distribution of tree cover conversion to other land uses in 2018 not followed by natural tree cover regrowth in 2019 to 2021. Circles represent locations of sample blocks identified as a particular conversion type using satellite imagery 3 years after the disturbance, and circle size is proportional to the area of that conversion type within the sample block. Global area estimates of all presented conversion types along with their standard errors are available in table S4. Class definitions and examples of satellite imagery are presented in (*17*). Constr., construction.

Comparison with the global drivers map

We compared [(*17*), table S8] our tree cover loss driver attribution results with the global map assigning the dominant driver of loss to the GTCL map pixels since 2001 (*9*) at 1-km resolution (*14*). In Africa, the global drivers map overestimates the extent of tree cover conversion to long-term agriculture (table S8). West Africa has highly heterogeneous small-scale land use dynamics, and assigning a single dominant "conversion to long-term agriculture" driver for 24 years of tree cover loss obscures rotation of existing tree plantations and shifting cultivation within 1-km grid cells (fig. S10). Additionally, the global drivers map assigns the driver of loss up to the most recent year (at the time of this study, 2024), not including a postdisturbance observation period, which may lead to confusion between tree cover loss associated with shifting and long-term agriculture.

In South and Southeast Asia, the global drivers map (*14*) incorrectly labels tree cover rotation within established palm plantations as "permanent agriculture," which is defined as "long-term, permanent tree cover loss for small- to large-scale agriculture" (*14*) and therefore should not include management of existing plantations (fig. S11). In our classification, nontimber tree plantation management, including palm, is excluded from the long-term conversion to agriculture (table S8).

The global drivers map in Latin America has high agreement with our results (table S8). Tree cover loss in this region is dominated by unidirectional conversion to predominantly treeless permanent agriculture (pasture and row crops), and thus, a single dominant driver of loss for 24 years, provided by the map at 1-km spatial resolution, reasonably characterizes individual years.

In North America and North and East Eurasia, forest fires and forestry operations are often colocated, for example, when previously logged forests burn or when salvage logging is happening after fires. This leads to a difference in the estimated proportion of fire- and forestry-related tree cover loss (table S8) in our single-year study versus using 24-year driver labels from the global map.

Discussion

The current analysis uses high-resolution satellite data (3 to 10 m) and a detailed classification legend (Table 1) to produce statistically rigorous area estimates of global tree cover loss drivers. Sample-based area estimation is a recommended good practice approach, as opposed to map pixel counting, which is affected by map errors (*34*, *35*). Although our approach is time-consuming, leading to a lag in producing estimates, it provides in-depth thematic insights from a comprehensive classification of a limited number of sample blocks rather than mapping a limited number of classes globally. This analysis can be replicated for future years, globally or for any geographic region, and for any land cover class of interest, with the main costs being the acquisition of commercial satellite data and the labor associated with creating high-quality sample block reference maps (*17*).

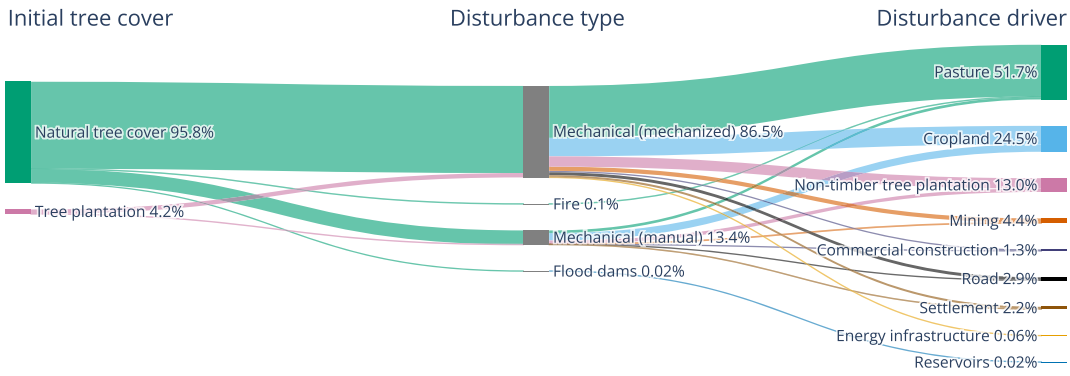

Fig. 5. Global tree cover conversion to other land uses in 2018 not followed by natural tree cover regrowth in 2019 to 2021. Link width is proportional to the area of each individual disturbance type and disturbance driver. Percent values are relative to the total area of tree cover conversion. Estimates of the absolute area of each conversion type and its contribution to the total area of tree cover loss (expressed as percentage) are presented in table S5. Class definitions and examples of satellite imagery are presented in (*17*).

Table 1. Attribution legend: Tree cover loss type and driver and predisturbance tree cover type assigned to each mapped pixel of tree cover loss within each sample block. For the specific definitions of terms used below, please refer to (*17*).

Predisturbance tree cover type		Disturbance type		Disturbance driver (proximate cause)
Natural tree cover		Mechanical clearing	■ Mechanized	■ Forestry – clearcut with natural regeneration
Tree plantation	■ Timber		■ Manual	■ Timber tree plantation or planted clearcut
	■Nontimber	Flooding due to dam construction		■ Selective logging, including timber tree plantation thinning
	■ Palm	Fire		■ Nontimber tree plantation (rubber, almond, cashew, etc.)
		Natural disturbances	■ Floods, including river meandering	■ Palm plantation
				■ Shifting agriculture
			■ Insect infestations	■ Long-term cropland
			■ Hurricanes and windfalls	■ Pasture
				■ Settlement
			■ Other (landslides, earthquakes, droughts, etc.)	■ Commercial construction
				■ Road
				■ Mining
				■ Energy infrastructure
				■ Flooded areas from dam construction
				■ Fire
				■ Natural disturbances, with subtypes matching those listed in Disturbance type
				■ Clearing with uncertain purpose

Limitations

Although we strived to produce the best possible reference map for each sample block and performed multiple quality checks (*17*), our results are affected by the following limitations. Our estimates are sample based (not a global map); the depth of regional analysis is limited by the sample size. Tree cover loss mapping was limited to 2018 and did not characterize long-term trends or interannual variability of loss driver areas. We considered land use 3 years after the disturbance to define tree cover loss drivers, which does not capture longer-term land use, e.g., conversion of tree cover to cropland with pasture as an intermediate step (*27*). The stratification that we used was based on the GTCL map (*9*), which misses some late 2018 disturbances, particularly fires and insect damages; therefore, our area estimates for these classes are likely somewhat conservative. Mechanized and manual mechanical clearing types were differentiated using contextual information (clearing size, presence of access roads) as opposed to tree cover loss mapping and differentiation of mechanical clearing from burning and inundation, which were based on satellite imagery signal and thus were more objective. Absence of very high–resolution data on Google Earth in the boreal region and persistent cloud cover in the tropics contributed to the varying quality of reference maps in space (fig. S12A) and the varying confidence of driver attribution (fig. S20). PlanetScope data has a limited number of spectral bands compared with Sentinel-2 data, and we acquired only one minimally cloudy PlanetScope image per month for each sample block to reduce data costs. We relied on Sentinel-2 imagery for mapping some fires (e.g., fig. S9C), insect damages, hurricanes (e.g., fig. S8G), and winter forestry, resulting in varying actual resolution of reference block maps.

Materials and Methods

I. Sampling design and analysis

To estimate the global extent and drivers of tree cover loss for the year 2018, we employed a one-stage cluster stratified random sampling design. The choice of cluster sampling design is motivated by reducing the cost of acquiring PlanetScope imagery (see section II 'Reference satellite data' below). The primary sampling unit was a 5x5 km block of 0.000025° (circa 3 m at equator) pixels. The choice of the block size was guided by the following considerations: minimizing the effort to produce reference maps for each sample block and covering each block with a minimum number of PlanetScope scenes to reduce mosaicking, while keeping the block size large enough to capture landscape-scale patterns of tree cover loss and target potential errors of omission in the map used for stratification (*9*), which are likely located in proximity to mapped tree cover loss.

The sampling population was constructed in geographic coordinates, with block boundaries aligning with the pixels from the 0.00025° (circa 30 m at equator) GLAD ARD raster grid (*36*). These blocks have the same number of pixels in the North-South dimension for all latitudes, but an increasing number of pixels in the East-West dimension closer to the poles to preserve near-equal block area (*37*). The resulting block population is near equal-area (maximum difference of block area compared to an equatorial block is 0.27%), and therefore to estimate the area we used estimators suitable for sampling from populations of equal-area units (*38*).

From the global grid of 5x5 km blocks, we excluded all blocks with <1% land surface as defined by the GADM world boundaries, version 2.0 (*39*). We have also removed blocks with zero percent of the year 2000 tree cover (*9*). The resulting sampling population consisted of 4,042,637 5x5 km blocks representing land areas with nonzero year 2000 tree cover.

One-stage cluster sampling means that all pixels within a block are assigned reference labels. We have created a sub-grid of 0.000025° pixels in geographic coordinates within each sample block, which corresponds to 3 m at the equator and matches the resolution of the finest reference data source used in the study (see section II 'Reference satellite data'). We used a separate supervised classification model for each sample block and iterated it in an active learning mode to assign reference labels to all pixels within each 5x5 km sample block cluster (see section III 'Tree cover loss mapping method').

Stratification was based on year 2018 global tree cover loss map (*9*), to concentrate the sampling effort in the areas of interest. To perform stratification, we computed percent of year 2018 tree cover loss from the map in each 5x5 km block in the population. We then subdivided the sampling population into four strata based on this percent tree cover loss. All the blocks with tree cover loss present were subdivided into two strata (high and low loss) based on the Dalenius-Hodges rule implemented in the R Stratification package (*40*). Resulting high and low loss strata contain roughly half of the mapped tree cover loss each, and percent per block tree cover loss threshold between the two strata is 3.3% (table S9). All the zero percent tree cover loss blocks in the population were split into two strata based on proximity to the mapped tree cover loss. The stratum representing 1-block buffer around blocks with detected tree cover loss (table S9) was meant to target potential areas of omission errors in the global tree cover loss map (*41*). Remaining blocks in the population (outside of the 1-block boundary) formed the no loss stratum. The resulting stratification is shown in fig. S1A.

The total number of sample blocks (600) was selected based on the feasibility to process reference data for, create reference block maps and attribute the drivers of tree cover loss within the 3-year project timeframe and available funding. We decided to select most blocks (500) from the two tree cover loss strata, as we have expected to find minimal tree cover loss area in the sample blocks with zero tree cover loss detected in the global Landsat-based map (*9*). We used Neyman optimal allocation (*40*) to allocate the 500-block sample among the two loss strata, resulting in 237 and 263 sample blocks in the high and low loss strata, respectively (see table S9). We have performed equal allocation of the remaining 100 blocks among the no loss and buffer strata (50 blocks each). The resulting sample of 600 5x5 km blocks is shown in fig. S1B.

To produce sample-based estimates of the tree cover loss area along with their standard errors, we used stratified estimators from (*38*), Eqs. 3, 25, and 26 with y_u defined as proportion of sample block u identified in the reference classification as tree cover loss. The target parameter y_u was redefined accordingly for each sample block to estimate the area of each tree cover loss driver class. To estimate percent of different disturbance types and drivers from the total area of tree cover loss (presented in tables S2 to S5) we employed the ratio estimator from (*38*), as both the numerator (area of an individual disturbance type or driver) and the denominator (total area of tree cover loss) are estimated from the sample. For the ratio estimator and its standard error [Eqs. 27 to 29, (*38*)], y_u is defined as proportion of sample block u identified as tree cover loss of a particular disturbance type or driver, and x_u as a proportion of sample block u identified as any tree cover loss.

Estimates were also produced for a set of reporting regions (table S1 and fig. S2). Each 5x5 km block in a population was assigned to a single region or climate domain. 'Climate domains' represent the aggregation of climate domains and a tropical rainforest ecoregion from the FAO Global Ecological Zones 2010 (*42*). Region boundaries are aggregated from the GADM country boundaries, version 2.0 (*39*). Each 5x5 km block was first assigned to the region or climate domain, which contained that block's centroid. Second, blocks for which the centroid did not fall into any region or climate domain (coastline blocks) were assigned to a particular region or climate domain if any part of the block intersected with that region or climate domain.

II. Reference satellite data

We used two primary sources of satellite imagery for producing reference tree cover blocks for each sample block: PlanetScope (3 m spatial resolution) and Sentinel-2 (10-20 m spatial resolution) optical images.

PlanetScope 4 band data were purchased from Planet Labs PBC through the National Aeronautics and Space Administration's (NASA's) Commercial SmallSat Data Acquisition (CSDA) program that provides access to commercial imagery for the NASA-funded research projects. To minimize the purchase of the PlanetScope data, which has daily global coverage, we have performed API searches to identify one minimally cloudy image per month for each sample block between December 2017 and February 2019. We started with zero percent cloud cover, and increased searches by 10% cloud cover increments. In case no zero percent cloud cover was available for a particular sample block in a particular month, we downloaded multiple partially cloudy images. Acquiring one minimally cloudy or multiple partially cloudy images in each month was aimed at capturing tree cover loss as it happens within the year, as in some cases, low intensity disturbances, such as selective logging in the tropics, might be obscured by the end of the year by understory regrowth. Our study period is calendar year 2018, but we have added imagery from December 2017, and January - February 2019 to better capture the timing of disturbances that occurred close to the start and the end of the study year. From all 600 sample blocks, the minimum number of acquired PlanetScope images per block was 10, the maximum was 224, with a median of 38 images per block.

Sentinel-2 data are available for free from the European Space Agency, and therefore, we acquired all available Sentinel-2 imagery between December 2017 and February 2019 for each sample block. Sentinel-2A and 2B combined have a revisit time of 5 days, so in our study, Sentinel-2 data had higher temporal resolution than acquired imagery from PlanetScope. From all 600 sample blocks, the minimum number of acquired Sentinel-2 images per block was 79, the maximum was 1024,

with a median of 174 images per block. We used all 10 m and 20 m bands of Sentinel-2 (Bands 3-8, 8A, 11 and 12).

All downloaded PlanetScope and Sentinel-2 imagery for each sample block was resampled to the common 0.000025° (circa 3 m) pixel grid in geographic coordinates, using the nearest neighbor resampling method. If a sample block was covered by more than one PlanetScope image within the same day (partial coverage by multiple scenes), a simple mosaicking was performed. The same was done for the Sentinel-2 imagery. All resampled and mosaicked imagery was combined into a single data stack for each block. No cloud masking was performed, as an individual classification model was built for each 5x5 km sample block, and at that spatial scale, clouds can simply be trained out from the final classification result.

In addition to individual PlanetScope 4-band scenes that were downloaded for block mapping, we used monthly PlanetScope basemap mosaics for visual interpretation of tree cover loss drivers for the years 2019 – 2021 (up to 3 years after the end of 2018). Monthly mosaics have slightly lower resolution (4.77 m) than the original imagery (3 m). We have accessed PlanetScope mosaic via a Planet QGIS plugin through an institutional license. A free version of the mosaics is available in the tropics, provided by the Norway's International Climate & Forests Initiative (NICFI) program, but the use of these free mosaics for the current project was limited by their geographic extent (tropical vs. global focus of the current study) and by their temporal availability (only by-annual mosaics are available prior to September 2020).

We have also utilized available very high-resolution (circa 1m or finer) imagery from Google Earth as a supplemental source of information while training tree cover loss models for each block and assessing resulting maps, and while assigning the drivers of tree cover loss. For block mapping, the primary use of high-resolution imagery from Google Earth was to verify that vegetation disturbances mapped with PlanetScope and Sentinel-2 data occurred within tree cover that has reached 3-5 m in height. The presence and extent of tree crown shadows in high-resolution imagery in sparse woody vegetation was a primary guide for distinguishing between shrubs and tree cover in uncertain cases. High resolution imagery, geotagged ground photographs and map labels available in Google Earth were also used as a supplementary source of information to identify tree cover loss drivers (fig. S19).

In addition to high-resolution data, we have also used 30-m resolution 16-day and annual composites of Landsat data from the UMD GLAD Analysis Ready Data (GLAD ARD, (*36*)) for the years 2017 – 2021. These data provided information from the year prior to mapped tree cover loss (2017) and three years after (2019 to 2021), which provided additional spectral information for the neighboring years in addition to the 4 spectral bands available in the PlanetScope basemaps. Landsat data were used in difficult cases to inform tree cover loss mapping, e.g., to verify that insect damage mapped in 2018 resulted in canopy loss, and not only in temporary defoliation. Landsat data were also used to aid tree cover loss driver attribution, e.g., to distinguish between long-term and shifting agriculture, or between conversion to cropland and pasture.

We also used 30-m resolution Harmonized Landsat-Sentinel-2 (HLS) data (*43*) for 2017 and 2018 to verify the sample blocks for which the global tree cover loss map detected 2018 loss, and our current study did not. Most of these cases represented late 2017 disturbance events, not adequately represented by the Landsat time series alone.

III. Tree cover loss mapping method

Each 5x5 km sample block was classified independently from other sample blocks into two classes: 'tree cover loss' and 'no tree cover loss'. Classification was performed using the classification and regression trees (CART) algorithm (*44*) in an ensemble learning mode with 15 individually trained trees combined via bootstrap aggregation (bagging). To train each tree, 15% of the training data within each block was randomly sampled. The block mapping was iterative, performed in an active learning mode: training data were modified following the results of each classification iteration until a satisfactory tree cover loss map was created for each block (see the next session for the map quality assessment procedure). Limited manual editing of the resulting reference maps was performed to eliminate persistent noise.

Training data for block classifications were produced using visual interpretation of the combined PlanetScope and Sentinel-2 data stack. As no cloud masking was performed, the clouds in the imagery were ignored during training data collection. By training on the cloudless parts of the image time series, each blocks' model was trained to ignore cloud cover.

Within each block, we mapped tree cover loss events that occurred between January 1 and December 31, 2018. We defined tree cover loss as removal of woody vegetation with a height exceeding 3-5 m. We did not employ a minimum patch size to define tree cover loss, so even a removal of an individual tree detectable in PlanetScope imagery was considered tree cover loss. Block 9 (*45*) represents an example of two separate stand-alone trees lost to river meandering in Ethiopia and detected as tree cover loss. However, only larger standalone trees, with crowns the size of multiple PlanetScope pixels would be detected in the current study as tree cover, e.g., larch trees with narrow crowns (<3x3 m) forming sparse tree cover in forest-tundra of Central and Eastern Siberia will not be detected as tree cover in the current study.

The fine spatial resolution of PlanetScope imagery helped outline the precise spatial extent of tree cover loss events, while the higher temporal resolution of acquired Sentinel-2 imagery was used to pinpoint the date of onset for each identified loss event. The temporal dimension was especially important around the start and end dates of the study period, because any tree cover loss occurring before 1 January and after 31 December 2018 was disregarded when collecting the training data.

To verify that we did not include temporary defoliation events (e.g., resulting from insect damage or droughts) in our tree cover loss maps we consulted 16-day GLAD ARD Landsat composites for the next season of the next 3 years (2019 to 2021) to verify that tree cover loss persisted and was not temporary.

IV. Quality checks of reference block maps and mapping confidence

The mapping team consisting of 4 to 6 people at a time was meeting roughly every two weeks during the 1.5-year mapping stage of the project. Each interpreter was presenting preliminary mapping results for each sample block they were assigned via displaying the GIS project with all the input imagery, training layers and preliminary classification results on a large screen. All members of the mapping team then reviewed the preliminary results together to identify areas that needed further improvement before the next quality assessment meeting or decided that the reference tree cover loss map for that sample block did not need any further improvement and could be considered finalized. The following three quality checks were performed systematically for each sample block.

Commission error check 1: Check for trees: This is a check for commission error resulting from incorrectly mapping tree cover loss in the areas that did not have tree cover at the beginning of the mapping period (1 January 2018). Example of this error is mapping burn scars in shrubland areas as tree cover loss. To perform this check, the least cloudy image or images closest to the start of the year and in some cases – additional imagery from the previous growing season were visually reviewed for the areas marked as tree cover loss in the preliminary mapping results to verify presence of tree cover prior to mapped disturbance.

Commission error check 2: Check for loss: This is a check for commission error resulting from incorrectly mapping tree cover loss in the areas that did not experience tree cover loss within the study period. Example of this error is mapping a temporary disturbance like understory

fire or temporary defoliation that does not lead to loss of canopy (tree branches and trunks) as tree cover loss. For this check, the least cloudy image or images closest to the end of the year (31 December 2018) and, in some cases, additional imagery from the next growing season were visually reviewed for the areas marked as tree cover loss in the preliminary mapping results to verify absence of tree cover following mapped disturbance.

Omission error check: Check for unmapped loss: This is a check for omission error resulting from not capturing some portion of tree cover loss within the sample block in the preliminary mapping results. Example of this error is omitting a certain type of disturbance from the training dataset leading to that disturbance type not being captured in the classification. To perform this check, the first and the last minimally clouded image(s) were visually compared in the areas marked as no tree cover loss in the preliminary mapping results to identify any potential areas where tree cover loss was initially missed.

Resulting map confidence: 'No loss' or 'loss' trainings were added in identified areas with commission or omission error (respectively) during the quality assessment meeting or after the meeting by the mapper responsible for the block if the identified areas of errors were extensive. The overall goal was to produce the best possible reference map for each sample block with the available satellite data. However, in persistently cloudy areas in the tropics and in boreal regions with limited availability of growing season imagery, the resulting reference maps could still have sub-optimal quality. During the quality assessment meetings, we have assigned the quality of the final block reference maps using the High/Medium/Low quality ranking (fig. S12A): 60.1% of reference maps had high quality, 33.3% had medium quality, and 6.6% had low quality. For the blocks with no tree cover loss identified from the reference imagery we have assigned the confidence of the absence of tree cover loss (fig. S12B): 72.7% of the 'no tree cover loss' blocks had high confidence, 19.2% had medium confidence, and 8.1% had low confidence. The majority of blocks with low mapping confidence and low presence/absence of tree cover loss were located in the boreal region, which was partially due to the absence of high-resolution imagery on Google Earth to verify the initial presence of tree cover within the burn scars.

Resulting tree cover loss maps for each block are available in a form of web page visualizations (*45*) and as a permanent data archive (*46*). Readers are encouraged to verify the quality of the resulting maps by reviewing individual sample block web pages with previews of tree cover loss maps and associated quality flags. We have also provided block outlines in .kml and .shp formats enabling verification of mapping results in Google Earth or in Planet Explorer.

V. Tree cover loss type and driver attribution: Class definitions and identification criteria

Each pixel in the reference tree cover loss maps for each sample block was manually attributed to a pre-disturbance tree cover type, initial disturbance type, and disturbance driver [or 'proximate cause,' (*16*)] indicating intended land use (Table 1). Attribution was performed by a single expert consulting a group of regional experts identified in the Author contributions and Acknowledgements sections. Repeat attribution of tree cover loss pixels to driver categories by multiple independent interpreters would have been cost-prohibitive and logistically challenging. Hence, we selected a consultation approach, where a single person attributes clusters of tree cover loss pixels in reference maps to specific drivers via hand-drawing vector polygons after consulting with all available reference sources and regional experts.

The pre-disturbance tree cover type was attributed based on the PlanetScope or Google Earth imagery before the disturbance event, or post-disturbance imagery for the surrounding areas with the same vegetation type that did not experience tree cover loss in 2018. Initial disturbance type was identified from the PlanetScope imagery right after the disturbance, and disturbance driver - from the monthly PlanetScope basemaps for the 3 years after the disturbance (2019 to 2021). The three-year window allowed to observe absence or presence of annual soil tilling to distinguish between tree cover conversion to cropland vs. pasture. It also allowed distinguishing between areas of shifting cultivation in the tropics that exhibit woody vegetation regrowth signal by the end of the 3-year period from the areas of long-term agriculture that do not have a regrowth signal. For tree plantation establishment, especially outside the tropics where tree growth is slower, the driver was primarily attributed from contextual information, e.g., presence plantation infrastructure or land use of the surrounding areas, rather than from the regrowth signal in PlanetScope basemaps, or, when available, from sub-meter resolution imagery from Google Earth.

Resulting tree cover loss type and driver labels can be viewed for each sample block at (*45*). When specific block numbers are mentioned as examples in the text below and in figs. S4 to S11 and S13 to S19, please refer to this web page.

Predisturbance tree cover type: The main distinction in pre-disturbance tree cover type identified in the study is tree plantations vs. natural tree cover (Table 1). We were looking for the signs of tree plantations, such as uniform canopy texture, regular shape of patches and road infrastructure in PlanetScope imagery, and trees of the same species planted in rows in sub-meter resolution imagery on Google Earth. Natural tree cover is therefore defined by excluding the opposite, i.e., by making sure the tree cover is not planted. Defined as such, natural tree cover includes any naturally regrowing woody vegetation that has reached 3-5 m in height, regardless of the physiognomy of trees, ecozone, seasonality, disturbance status, etc. Natural tree cover will also include forests planted in an irregular manner (hand planting), and forests that originated from seed dispersal (typical for managed boreal forest). We have avoided separating the natural tree cover into categories like forests vs. woodlands, or primary forests vs. secondary forests, because it is extremely difficult to come up with a valid global definition for these categories and consistently identify them via visual interpretation of <5 m satellite imagery.

Tree plantation class was subdivided into timber, non-timber, and palm plantations. Timber plantations are monoculture stands of tree species primarily used for timber and wood pulp, such as pine, eucalyptus and acacia (Fig. S13). Non-timber plantations (Fig. S14) include rubber and tall orchards, with trees reaching over 3m when mature (e.g., cashew, almond). Short orchards (below 3m in height) where considered a part of the cropland class, and therefore any changes in the canopy of the short orchard were not considered tree cover loss. Mature oil palm plantations (Fig. S14) were considered tree cover. Assignment of the type of tree plantation was relying primarily on sub-meter resolution imagery in Google Earth, which is typically available in the developed areas with tree plantations. Geotagged ground photographs from Google Earth (Fig. S19A) helped increase the confidence of plantation type assignment. One area of thematic uncertainty in identification of tree plantations is West Africa, where small-scale plantations are common, and sub-meter satellite imagery and geotagged photographs are not always available. We have also likely mislabeled some of the mature timber tree plantations in the boreal region as natural tree cover due to the absence of sub-meter imagery. Results for palm plantations are reported combined with other non-timber tree plantations in the manuscript; palm plantation labels separate from other non-timber tree plantations are available in the sample-block-level results table (*46*).

Initial disturbance type: Initial disturbance type was identified from the same PlanetScope imagery (December 2017 to February 2019, individual scenes) that was used for mapping tree cover loss. We have identified how the tree canopy cover was lost (Table 1 and Fig. 2): through mechanical

canopy removal by humans or via inundation from dam construction, by fire, or due to natural disturbances (windfalls and hurricanes, floods and river meandering, insect infestation, landslides, earthquakes, etc.). Examples of sample blocks with fire and natural disturbances are presented in fig. S15. We did not separate fires into human-caused and naturally ignited (e.g., from lightning strikes), as it is not possible to do using satellite imagery alone. Fires included tree cover loss occurring directly as a result of fire; slash-and-burn agriculture, which includes burning of the felled trees, is included into the 'mechanical clearing' category. We mapped only the pixels that experienced tree cover loss, and therefore only the parts of the burn scars that had trees before the fire are included (fig. S15A). Windfalls and hurricanes were confirmed via the presence of felled trees following the hurricane path in sub-meter imagery on Google Earth, when available. We have also gathered additional information via Google searches to verify prominent natural disturbances, e.g., 2018 Siberian silkmoth infestation in Tomsk, Omsk and Krasnoyarsk regions of Russia (blocks 369, 410, 412, 576 and 472, fig. S15B), hurricane Michael damage on the boundary between Florida and Georgia, USA (block 510, fig. S8, E to H) or storm David in Germany (block 522, fig. S13C). We used imagery from 3 years after the disturbance to confirm that the mapped extent of natural disturbances represents persistent tree cover loss signal and not temporary defoliation. No major floods are detected in the study. Examples of limited tree cover loss due to natural flooding and river meandering are blocks 199 and 345, and flooding due to dam construction (ponds) – blocks 438 and 539.

Mechanical tree cover clearing by humans was subdivided into mechanized (fig. S16) and manual (non-mechanized, fig. S17). These sub-categories were deduced from the clearing size (larger clearings correspond to mechanized clearing), shape (sharper clearing edges and uniform clearing shapes correspond to mechanized clearing) and presence of access roads for heavy machinery. Mechanized clearing presumes the use of heavy machinery (skidders, feller bunchers, harvesters) and trucks; using hand-held chainsaws as the only mechanization of clearing is considered manual clearing, as it cannot be reliably distinguished from purely non-mechanized clearing (with axes) from space.

Disturbance driver (proximate cause): Disturbance driver or proximate cause of tree cover loss (*16*) was attributed based on the land use 3 years after the disturbance, observed in the satellite imagery. Disturbance driver categories used in the study are listed in Table 1. For the reporting (Fig. 3), we have combined these land use-based driver categories with pre-disturbance tree cover types to come up with broader driver categories. For example, if land use 3 years after the disturbance indicates 'non-timber tree plantation', it was classified as 'non-timber tree plantation management' (Fig. 3B) if the detected tree cover loss occurred in the existing non-timber tree plantation. At the same time, if non-timber tree plantation is replacing natural tree cover or timber tree plantations, then it was classified as conversion to other land uses (Figs. 3E and 4C).

The first group of drivers (Fig. 3, B and D) covers forestry operations in natural tree cover and timber tree plantation management (fig. S18). We distinguished between clearcuts (including harvesting of timber tree plantations) and selective logging (including timber tree plantation thinning). Forestry operations were marked as selective logging or thinning if tree cover in less than 50% of the logging extent was taken out. Roads in selective logging landscapes were included as a part of logging damages and not as conversion of tree cover into road infrastructure (fig. S18B). Clearcuts were separated into clearcuts with natural regeneration (in natural forests) and planted clearcuts (replacing natural forests or re-establishment of a tree plantation after harvesting). Planted clearcuts in the boreal region were attributed based on the neighboring older clearcuts, as tree cover regrowth in the boreal region is slow and the regrowth signal in the imagery 3 years after the disturbance is not confidently distinguishable from clearcuts with natural regeneration. Roads within clearcuts were included into forestry; more permanent roads between clearcuts – classified as conversion of tree cover into road infrastructure (fig. S18C).

Tree cover rotation in a shifting agriculture cycle (Fig. 3C) was identified from the spatial pattern of small- and medium-sized clearings (fig. S17, A and B) that do not have an annual bare ground signal consistent with soil tilling typical for long-term agriculture, and that exhibit a signal of shrub and/or tree cover regrowth at the end of the 3 years after the disturbance. Longer fallows (4 years or longer) where we see tree cover regrowth between clearings are included into the 'shifting agriculture' class, even if the area is always under cultivation and in that sense closer to long-term agriculture (e.g., Block 571 in Nigeria).

For natural disturbances (Fig. 3E) disturbance driver corresponds to the initial disturbance type, described in the previous section. Tree cover loss pixels with initial tree cover loss due to fire were classified as "wildfires" (Fig. 3E and table S3) if no productive land use was observed 3 years after the fire. Out of 37 blocks, which had all or part of tree cover loss classified as loss due to fire, only 1 had a productive land use 3 years after (pasture, block 550 in Guatemala), resulting in a very small area of conversion to pasture by fire (Fig. 5 and table S5).

Conversion of tree cover to other land uses (Figs. 3A and 4) included conversion of any tree cover to long-term cropland, pasture, settlements, commercial construction, roads, mining sites, reservoirs and energy infrastructure, and conversion of natural tree cover or timber plantations into non-timber tree plantations (including tall orchards). Conversion to pasture (Fig. 4A) was identified via the presence of animal trails and watering holes in PlanetScope imagery, and absence of annual tilling signal to distinguish pastures from croplands. In some cases, we were able to verify pasture land use by the presence of livestock in sub-meter imagery on Google Earth (Blocks 327, 384, 474, fig. S19C).

Conversion to long-term (permanent) cropland (Fig. 4B) included annually tilled agricultural fields and short fallows replacing tree cover, with at least one re-clearing observed between the initial tree cover loss in 2018 and the end of 2021. Longer fallows replacing tree cover were classified as shifting agriculture (Fig. 3C). Long-term cropland includes short orchards (under 3m tall). Hayfields (e.g., fig. S19B) are included in a long-term cropland class if there is tilling (bare ground) signal, i.e., grasses are planted at least once in the 3 years after the disturbance.

Conversion to non-timber tree plantations (Fig. 4C) included non-timber tree plantations and palm plantations replacing natural tree cover and timber plantations. See section 'Pre-disturbance tree cover type' above for the types of plantations included in non-timber tree plantation class, and their identification criteria.

Conversion to roads (Fig. 4D) included tree cover being replaced by roads, both paved and persistent unpaved roads (not temporary paths). Conversion to roads excluded roads within clearcuts and within selective logging landscapes (fig. S18B); those were classified as forestry/clearcut and selective logging, respectively. More permanent roads between clearcuts likely to be used in the future for through-traffic (between clearcuts or for other purposes) were classified as conversion to roads (fig. S18C). The same logic applied to mining sites: roads within mining sites likely to use only to service the mines were included in the mining class, and new roads between mining sites were included into conversion to roads.

Conversion to energy infrastructure (Fig. 4D) included tree cover replaced by power lines (Blocks 252 and 334) and windmills (Block 324). We did not encounter other types of energy infrastructure (e.g., oil and gas pipes) replacing tree cover in our sample, but they would have been included in this class as well.

Conversion to mines (Fig. 4D) was identified via the presence of persistent bare ground, often surrounding rivers (e.g., in artisanal gold mining). Presence of mining infrastructure in high resolution imagery and ground geotagged photographs on Google Earth, as well as the names of mines helped verify identification of industrial mining sites (fig. S19D).

Conversion to settlements (Fig. 4D) included built-up areas with residential land use replacing tree cover, while commercial construction included non-residential built areas. Greenhouses and telecommunication infrastructure (towers) were included in commercial construction.

Finally, clearing with uncertain purpose (Fig. 3F) included those cases, in which tree cover was likely converted to non-treed land use, but the exact driver of the conversion was not clear. This is a thematically uncertain class, some portion of which corresponds to land grabbing (land banking). Most of the area identified as a clearing with uncertain purpose is in Brazil and Indonesia, two known hotspots of land grabbing. In Indonesia, these blocks are likely associated with banking/land grabbing practices, in which the land is left idle (without a productive land use) for a number of years after the initial clearing (*26*). In Brazil, land grabbing is mostly associated in the literature with the frontier of deforestation and establishing pastures as a way of demonstrating productive land use for registering the claimed land (*47*), with a significant proportion of that claimed land later converted to cropland land use (*27*, *48*). In our study such land grabbing would have likely been classified as 'conversion to pasture', and the 'uncertain purpose' blocks in Brazil are mainly located outside of the deforestation frontier, typically close to settlements or established tree plantations. This is a relatively rare class in terms of its contribution to the global tree cover loss (table S3) and cannot be quantified with high precision from our limited global sample of 600 blocks.

VI. Confidence of tree cover loss type and driver attribution

During the visual assignment of tree cover loss type and driver to all patches of mapped tree cover loss within each block, we have assessed confidence (high, medium, low) of each unique combination of pre-disturbance tree cover type (natural forests, timber- and non-timber tree plantations), initial disturbance type (Fig. 2) and disturbance driver (Figs. 3 and 4) at the sample block level. Proportion of blocks of each confidence level in the combined tree cover loss driver categories is shown in fig. S20.

'Clearing with uncertain purpose' is an inherently thematically uncertain class, and therefore all pixels labeled as such have low confidence of tree cover loss type. From all other categories, the categories with the highest proportion of high and low confidence blocks are 'Natural disturbances' and 'Wildfires'. Medium confidence category is relatively rare in these categories, because for these tree cover loss types the initial disturbance type and driver of disturbance are the same, and therefore there are fewer dimensions for thematic uncertainty. At the same time, high proportion of low confidence blocks within these categories compared to tree cover clearing reflects that the signal associated with natural disturbances and wildfires in the satellite imagery is fuzzier and more transient. Also, natural disturbances and wildfires often happen in remote areas, where high resolution satellite imagery and geotagged photographs on Google Earth are not available.

Larger proportion of medium confidence sample blocks in the forestry in natural forests, shifting agriculture and conversion classes (fig. S18) is partially due to the difficulties in distinguishing between mechanized and manual clearing types (see section V above and figs. S16 and S17). Confidence of forestry sample blocks labeling is also affected by the uncertainty related to whether the clearcuts were planted afterwards or left to regrow naturally. Medium and low confidence shifting agriculture blocks correspond to the areas with likely confusion with small-scale forest conversion to non-timber tree plantation (rubber, palm) and long-term agriculture. Conversion blocks with lower confidence reflect potential confusions between conversion classes (e.g., between conversion to cropland and pasture).

VII. Comparison with the global tree cover loss map

Comparison of the current results with the global tree cover loss map (*9*) presented in the main text, table S7, and figs. S4 to S9 should be considered in the light of the following methodological caveats.

Differences in tree cover definitions: Global tree cover loss map (*9*) maps any loss of tree cover taller than 5 m at the 30 m resolution, not imposing any percent tree cover threshold. This means that some of the detected tree cover loss could be in areas with very low percent tree cover, e.g., under 10%. Even 10% tree cover at the 30m resolution could mean 10 trees with 3x3 m crowns (one PlanetScope pixel each) spread out within the 30 m pixel, with large gaps in between. In our current study during visual interpretation of PlanetScope (3 m) and Sentinel-2 data we would not be able to identify such sparse tree cover of trees with smaller crowns not readily distinguishable in 3 m resolution as tree cover, especially in the absence of very high resolution (1 m) imagery on Google Earth, which is often the case in the boreal forests of Central and Eastern Siberia. Hence, we observed substantial differences between the area of tree cover loss mapped in the current study and in the global tree cover loss map for the fire blocks in Russia (figs. S6A and S9): for these blocks the entire area mapped by the global tree cover loss did burn in 2018, but it is unclear and impossible to verify in the absence of very high resolution imagery the presence of tree cover. Our current study likely represents a conservative estimate of tree cover loss area for those blocks, and for other open-canopy ecosystems, such as tropical and subtropical dryland shrublands and dry forests.

Errors in date attribution for disturbances close to the end of the year: Global tree cover loss map (*9*) detected some late-year 2017 disturbance events (fires, clearcuts, logging, insect damages) as year 2018 loss. We have reviewed sample blocks for which the global map mapped some tree cover loss in 2018, and the current study did not (shown in black in figs. S4 to S6), and were able to assign late-year 2017 loss as the source of disagreement in most cases. Based on this analysis, late-year 2017 tree cover loss included in the global map as 2018 loss accounts for at least 17,000 km^2 globally: ~12,700 km^2 in the boreal region (or 27% of the difference between the map and the current study), ~2,500 km^2 in the temperate region (or 34% of the difference) and ~3,000 km^2 in the tropics (although in the tropics the estimates from the current study are still higher than the global map). The contribution of late 2017 loss mapped as 2018 in the global map is not that large at the global scale (only about 6% of the mapped loss), but is more pronounced at the regional and national levels, particularly – in boreal and temperate regions, in Russia and the United States (figs. S4 and S6).

The delay of tree cover identification in the global tree cover loss map is documented in the original paper (*9*), which reports the mean absolute deviation of the loss date of 0.29 years (validated by the MODIS time-series data). This means that some of the late-2018 tree cover loss in the map is mapped as 2019 loss although we could not quantify the extent of it in the current study. For example, fig. S8, E to H, represents an example of late 2018 hurricane damages not fully picked up by the global map in that year. We used the year 2018 map to target our sampling effort in the current study: the 5x5 km resolution sampling strata were defined based on the presence of 2018 tree cover loss in the global map. Consequently, our stratification does not target potential late-2018 tree cover loss spatially isolated from all other 2018 loss (e.g., fires in remote areas), and the sample-based estimate of tree cover loss in the current study is likely somewhat conservative. In other words, for disturbance drivers that are likely to occur in remote areas, such as fires, hurricanes and other natural disturbances, our current sample-based estimate might be underestimating the true area affected by these drivers.

Difference in mapping repeated tree cover loss events: Global tree cover loss map (*9*) detects only the first tree cover loss event since 2001. This means that some proportion of tree cover loss we detected in the current study as 2018 loss has been cleared sometime between 2001 and 2017, then has regrown and was cleared again in 2018. This is less likely to happen in the boreal and temperate regions, where the rate

of tree cover regrowth is slow. In the tropical and subtropical regions, where tree cover regrows quickly, such repeated loss is more likely. To estimate the contribution of this effect to the disagreement between the sample and the map, we have subtracted all 2001 to 2017 tree cover loss from the reference block maps produced in the current study. This improved the agreement between the map and the current study in Tropical Rainforests (from $R^2 = 0.49$ to 0.60), Subtropical domain (from $R^2 = 0.65$ to 0.74), in Africa (from $R^2 = 0.35$ to 0.39) and in South and Southeast Asia (from $R^2 = 0.59$ to 0.74), and in the Democratic Republic of the Congo (from $R^2 = 0.67$ to 0.74) and Indonesia ($R^2 = 0.61$ to 0.85). Substantial improvement of agreement in the Temperate domain (from $R^2 = 0.70$ to 0.78) was due to removal of repeated loss from one fire block. The rest of the climate domains, continents and major countries in figs. S4 to S6 showed only minor changes in agreement (R^2 change of 0.03 or smaller).

For nonmechanized shifting cultivation blocks, removal of repeated loss resulted in substantial change of the reference loss values, but the agreement is still low (changed from $R^2 = 0.26$ to 0.28), which means that the differences in mapping the small-sized clearings in 30 m versus 3 m resolution are the main source of disagreement. We have visually inspected the intersection of the global map, and the reference block maps produced in the current study for several block maps and confirmed that location of individual clearings and the overall clearing pattern match well between the two data sources, and the area differences are mainly coming from the mixed pixels on the boundaries of clearing patches in the 30 m resolution global map.

Fire was the only driver from fig. S7 that exhibited substantial improvement of agreement (R^2 change larger than 0.03) when repeated loss was removed (from $R^2 = 0.35$ to 0.40), indicating repeated tree cover burning or other disturbances (e.g., selective logging or plantation management) followed by fire, sometimes – years later. In some cases, forest fires detected by the global map in 2001 to 2017 might not have experienced tree cover loss in parts of the burn scar, and repeated burning in 2018 might have led to loss of these remaining treed areas. In other cases, there might have been tree cover regrowth after early 2000s fire, and then repeated burning of that regrowth.

VIII. Comparison with the global drivers map

Comparison of the current results with the global tree cover loss drivers map (*14*) presented in the main text, table S8 and in figs. S10 and S11 included the following steps. We have excluded 2000 to 2017 tree cover loss detected by GTCL map from our reference block maps for the purposes of this comparison, and attributed loss drivers to only 2018 GTCL pixels using the global drivers map (*14*). We have also aggregated the driver classes from our study (Table 1) to ensure a close match with the classes from the global drivers map (table S8). The remaining caveat affecting the results of this comparison is that the global drives map assigns a single dominant tree cover loss driver for 2001 to 2024 within each 1km grid cell and thus does not capture the drivers that are not dominant in time or represent a minority class in space.

REFERENCES AND NOTES

1. P. Smith *et al.*, Competition for land. *Philos. Trans. R. Soc. Lond. B Biol. Sci.* **365**, 2941–2957 (2010). doi: 10.1098/rstb.2010.0127; pmid: 20713395
2. C. L. Giebink *et al.*, The policy and ecology of forest-based climate mitigation: Challenges, needs, and opportunities. *Plant Soil* **479**, 25–52 (2022). doi: 10.1007/s11104-022-05315-6
3. A. Kavvada *et al.*, Towards delivering on the Sustainable Development Goals using Earth observations. *Remote Sens. Environ.* **247**, 111930 (2020). doi: 10.1016/j.rse.2020.111930
4. M. A. Wulder, J. G. Masek, W. B. Cohen, T. R. Loveland, C. E. Woodcock, Opening the archive: How free data has enabled the science and monitoring promise of Landsat. *Remote Sens. Environ.* **122**, 2–10 (2012). doi: 10.1016/j.rse.2012.01.010
5. V. C. Radeloff *et al.*, Need and vision for global medium-resolution Landsat and Sentinel-2 data products. *Remote Sens. Environ.* **300**, 113918 (2024). doi: 10.1016/j.rse.2023.113918
6. X. P. Song, The future of global land change monitoring. *Int. J. Digit. Earth* **16**, 2279–2300 (2023). doi: 10.1080/17538947.2023.2224586
7. FAO, *FRA 2020 Remote Sensing Survey* (Food and Agriculture Organization of the United Nations, Rome, 2022; https://www.fao.org/documents/card/en/c/cb9970en).
8. V. Zalles, N. Harris, F. Stolle, M. C. Hansen, Forest definitions require a re-think. *Commun. Earth Environ.* **5**, 620 (2024). doi: 10.1038/s43247-024-01779-9
9. M. C. Hansen *et al.*, High-resolution global maps of 21st-century forest cover change. *Science* **342**, 850–853 (2013). doi: 10.1126/science.1244693; pmid: 24233722
10. C. Smith, J. C. A. Baker, D. V. Spracklen, Tropical deforestation causes large reductions in observed precipitation. *Nature* **615**, 270–275 (2023). doi: 10.1038/s41586-022-05690-1; pmid: 36859548
11. P. Borrelli *et al.*, An assessment of the global impact of 21st century land use change on soil erosion. *Nat. Commun.* **8**, 2013 (2017). doi: 10.1038/s41467-017-02142-7; pmid: 29222506
12. P. Friedlingstein *et al.*, Global Carbon Budget 2021. *Earth Syst. Sci. Data* **14**, 1917–2005 (2022). doi: 10.5194/essd-14-1917-2022
13. P. G. Curtis, C. M. Slay, N. L. Harris, A. Tyukavina, M. C. Hansen, Classifying drivers of global forest loss. *Science* **361**, 1108–1111 (2018). doi: 10.1126/science.aau3445; pmid: 30213911
14. M. J. Sims *et al.*, Global drivers of forest loss at 1 km resolution. *Environ. Res. Lett.* **20**, 074027 (2025). doi: 10.1088/1748-9326/add606
15. A. Tyukavina *et al.*, Global Trends of Forest Loss Due to Fire From 2001 to 2019. *Front. Remote Sens.* **3**, 825190 (2022). doi: 10.3389/frsen.2022.825190
16. H. J. Geist, E. F. Lambin, Proximate Causes and Underlying Driving Forces of Tropical Deforestation. *Bioscience* **52**, 143 (2002). doi: 10.1641/0006-3568(2002)052[0143:PCAUDF]2.0.CO;2
17. Materials and Methods.
18. Planet Team, Planet Application Program Interface: In Space for Life on Earth (2025); https://api.planet.com.
19. Copernicus Sentinel-2 data, 2017-2019 (CDSE); https://dataspace.copernicus.eu/data-collections/copernicus-sentinel-missions/sentinel-2.
20. H. Yang *et al.*, Climatic and biotic factors influencing regional declines and recovery of tropical forest biomass from the 2015/16 El Niño. *Proc. Natl. Acad. Sci. U.S.A.* **119**, e2101388119 (2022). doi: 10.1073/pnas.2101388119; pmid: 35733266
21. R. Seidl *et al.*, Forest disturbances under climate change. *Nat. Clim. Chang.* **7**, 395–402 (2017). doi: 10.1038/nclimate3303; pmid: 28861124
22. S. Turubanova, P. V. Potapov, A. Tyukavina, M. C. Hansen, Ongoing primary forest loss in Brazil, Democratic Republic of the Congo, and Indonesia. *Environ. Res. Lett.* **13**, 074028 (2018). doi: 10.1088/1748-9326/aacd1c
23. G. Molinario, M. C. Hansen, P. V. Potapov, Forest cover dynamics of shifting cultivation in the Democratic Republic of Congo: A remote sensing-based assessment for 2000-2010. *Environ. Res. Lett.* **10**, 094009 (2015). doi: 10.1088/1748-9326/10/9/094009
24. A. Tyukavina *et al.*, Congo Basin forest loss dominated by increasing smallholder clearing. *Sci. Adv.* **4**, eaat2993 (2018). doi: 10.1126/sciadv.aat2993; pmid: 30417092
25. P. E. Barni *et al.*, Logging Amazon forest increased the severity and spread of fires during the 2015–2016 El Niño. *For. Ecol. Manage.* **500**, 119652 (2021). doi: 10.1016/j.foreco.2021.119652
26. D. Parker *et al.*, Land in limbo: Nearly one third of Indonesia's cleared old-growth forests left idle. *Proc. Natl. Acad. Sci. U.S.A.* **121**, e2318029121 (2024). doi: 10.1073/pnas.2318029121; pmid: 38950360
27. V. Zalles *et al.*, Rapid expansion of human impact on natural land in South America since 1985. *Sci. Adv.* **7**, eabg1620 (2021). doi: 10.1126/sciadv.abg1620; pmid: 33811082
28. X. P. Song *et al.*, Massive soybean expansion in South America since 2000 and implications for conservation. *Nat. Sustain.* **2021**, 784–792 (2021). doi: 10.1038/s41893-021-00729-z; pmid: 34377840
29. F. Pendrill *et al.*, Disentangling the numbers behind agriculture-driven tropical deforestation. *Science* **377**, eabm9267 (2022). doi: 10.1126/science.abm9267; pmid: 36074840
30. D. L. A. Gaveau *et al.*, Slowing deforestation in Indonesia follows declining oil palm expansion and lower oil prices. *PLOS ONE* **17**, e0266178 (2022). doi: 10.1371/journal.pone.0266178; pmid: 35349594
31. X. Liu *et al.*, High-spatiotemporal-resolution mapping of global urban change from 1985 to 2015. *Nat. Sustain.* **3**, 564–570 (2020). doi: 10.1038/s41893-020-0521-x
32. V. Maus *et al.*, An update on global mining land use. *Sci. Data* **9**, 433 (2022). doi: 10.1038/s41597-022-01547-4; pmid: 35869082
33. L. Tang, T. T. Werner, Global mining footprint mapped from high-resolution satellite imagery. *Commun. Earth Environ.* **4**, 134 (2023). doi: 10.1038/s43247-023-00805-6
34. P. Olofsson *et al.*, Good practices for estimating area and assessing accuracy of land change. *Remote Sens. Environ.* **148**, 42–57 (2014). doi: 10.1016/j.rse.2014.02.015
35. A. Tyukavina *et al.*, Land Cover and Change Map Accuracy Assessment and Area Estimation Good Practices Protocol, version 1.1: Land Product Validation Subgroup (WGCV/CEOS, 2025); https://doi.org10.5067/doc/ceoswgcv/lpv/lc.001.
36. P. Potapov *et al.*, Landsat analysis ready data for global land cover and land cover change mapping. *Remote Sens. (Basel)* **12**, 426 (2020). doi: 10.3390/rs12030426
37. A. Tyukavina, S. V. Stehman, A. H. Pickens, P. Potapov, M. C. Hansen, Practical global sampling methods for estimating area and map accuracy of land cover and change. *Remote Sens. Environ.* **324**, 114714 (2025). doi: 10.1016/j.rse.2025.114714

38. S. V. Stehman, Estimating area and map accuracy for stratified random sampling when the strata are different from the map classes. *Int. J. Remote Sens.* **35**, 4923–4939 (2014). doi: 10.1080/01431161.2014.930207
39. GADM data; https://gadm.org/data.html.
40. L. P. Rivest, S. Baillargeon, Stratification: Univariate Stratification of Survey Populations, version 2.2-7 (R Project, 2022); https://doi.org/10.32614/CRAN.package.stratification.
41. P. Olofsson *et al.*, Mitigating the effects of omission errors on area and area change estimates. *Remote Sens. Environ.* **236**, 111492 (2020). doi: 10.1016/j.rse.2019.111492
42. FAO, Global ecological zones for FAO forest reporting: 2010 Update, Forest resources Assessment Working Paper 179 (Food and Agriculture Organization of the UN, 2012).
43. M. Claverie *et al.*, The Harmonized Landsat and Sentinel-2 surface reflectance data set. *Remote Sens. Environ.* **219**, 145–161 (2018). doi: 10.1016/j.rse.2018.09.002
44. L. Breiman, J. Friedman, R. A. Olshen, C. J. Stone, *Classification and Regression Trees* (Chapman and Hall/CRC, 2017).doi: 10.1201/9781315139470
45. A. Tyukavina *et al.*, Visualization of reference sample block maps; https://glad.umd.edu/Global_drivers/.
46. A. Tyukavina *et al.*, Global 5km sample blocks with 2018 tree cover loss and its drivers mapped using PlanetScope and Sentinel-2 data, Zenodo (2025); https://doi.org/10.5281/zenodo.17652508.
47. G. C. Carrero, R. T. Walker, C. S. Simmons, P. M. Fearnside, Land grabbing in the Brazilian Amazon: Stealing public land with government approval. *Land Use Policy* **120**, 106133 (2022). doi: 10.1016/j.landusepol.2022.106133
48. J. Graesser, T. M. Aide, H. R. Grau, N. Ramankutty, Cropland/pastureland dynamics and the slowdown of deforestation in Latin America. *Environ. Res. Lett.* **10**, 034017 (2015). doi: 10.1088/1748-9326/10/3/034017
49. A. Tyukavina, Archived code repository for the global drivers of tree cover loss study, Zenodo (2025); https://doi.org/10.5281/zenodo.17652863.

ACKNOWLEDGMENTS

We are grateful to C. Souza Jr. and P. Defourny for helping secure funding for this project. We thank H. M. Papagjika for participation in tree cover loss mapping; A. Adebayo, T. Nana, N. Hanh Quyen, M. Adami, and A. Lima for assistance in assigning drivers of tree cover loss; A. Panchenko for help selecting the boundaries of reporting regions; and M. Sims for help with the global drivers map comparison. **Funding:** This work was supported by the NASA Land Cover Land Use Change program (no. 80NSSC21K0308), the Bezos Earth Fund through the World Resources Institute (WRI) Land and Carbon Lab (no. G2436), the WRI Global Forest Watch program (no. G2601), and the NASA/United States Geological Survey (USGS) Landsat Science Team (no. 140G0118C0013). NASA's CSDA program provided access to PlanetScope data. **Author contributions:** Conceptualization: A.T., M.C.H., P.P., N.H.; Data processing: B.A., X.-P.S., A.K.; Tree cover loss mapping: A.J.P., A.B., C.O.D., A.M., A.O., W.B., S.P., L.T., A.I., J.P., A.T.; Assigning tree cover loss drivers: A.T., D.P., P.P., S.T., V.Z.; Training mapping team: J.P., A.T.; Quality assessment supervision: A.J.P., J.P.; Code and software: A.T., P.P., A.H.P.; Formal analysis: A.T.; Visualization: A.T., A.K.; Web design: Y.H.; Funding acquisition: A.T., M.C.H., P.P:, Writing – original draft: A.T.; Writing – review and editing: M.C.H., P.P., D.P., A.H.P., A.K., X.-P.S., J.P., V.Z. **Competing interests:** Authors declare that they have no competing interests. **Data, code, and materials availability:** All data produced in the current project required to reproduce the tables and figures and visualizations of the sample block reference maps are provided at (*45*) and archived at (*46*). The area estimation code used to produce area estimates presented in tables S1 to S5 is archived at (*49*). No new materials were created in this study. Source PlanetScope 4 band imagery (*18*) used to map 2018 tree cover loss for each sample block purchased for this project from Planet Labs PBC through NASA's CSDA program is available cost-free to NASA- and NSF- funded research projects and to US Federal civil agencies through the CSDA archive. For other researchers, the source PlanetScope 4 band imagery used in the current project is available from Planet Labs archive for purchasing. PlanetScope basemap mosaics used for loss driver attribution are publicly available only for the tropics through the NICFI program; outside the tropics the basemap mosaics are available only via a paid subscription. Sentinel-2 imagery used in the study is freely available to the public from Copernicus Browser (*19*). Source Landsat imagery is provided for free by the USGS; the version of the data used in this study (GLAD Landsat Analysis Ready Data) is also freely available (*36*).

SUPPLEMENTARY MATERIALS

science.org/doi/10.1126/science.adz9042
Figs. S1 to S20; Tables S1 to S9

Submitted 20 June 2025; accepted 18 March 2026

10.1126/science.adz9042